Int. J. Heat Mass Transfer. Vol. 22, pp. 611–623

0017-9310/79/0401-0611 $02.00/0

FREE CONVECTION IN THERMALLY STRATIFIED WATER COOLED FROM ABOVE

M. BEHNIA and R. VISKANTA
Heat Transfer Laboratory, School of Mechanical Engineering, Purdue University, West Lafayette, IN 47907, U.S.A.

(*Received* 21 *November* 1977 *and in revised form* 14 *July* 1978)

Abstract—The thermal and fluid kinetics of the convective layer during cooling from the free surface of a thermally stratified water by convection, latent energy transport, and radiation is studied. Laboratory experiments were performed and a Mach–Zehnder interferometer was used to measure the unsteady temperature distribution in a test cell filled with water which was previously stratified. A simple mathematical model based on a thermal energy balance is developed to predict the thickness and the mean temperature of the layer. The model predictions agreed to within 10% with the data from controlled laboratory experiments. It was found that the numerical solution to the model equations agree better with the experimental data than those based on the closed form analytical solution using the constant average surface heat flux. It was determined that the surface boundary condition and the internal physical processes of mixing and entrainment must be better understood in order to model the dynamics of the mixed layer in natural waterbodies.

NOMENCLATURE

- c, specific heat;
- C, constant defined by equation (14);
- g, mass-transfer coefficient;
- H, heat flux defined by equation (3);
- h, convective (mixed) layer thickness;
- $\tilde{h}$, effective heat-transfer coefficient defined by equation (11);
- h_c, convective heat-transfer coefficient;
- h_{fg}, latent heat of vaporization;
- k, thermal conductivity of water;
- p, partial pressure of water vapor;
- S, dimensionless temperature stratification parameter, $(\tilde{T}_a - T_{0i})/\delta\gamma_i$;
- T, temperature;
- T_e, effective environment temperature;
- T_a, effective ambient air temperature;
- T_o, initial water temperature;
- T', fluctuating temperature;
- w', fluctuating vertical velocity component;
- z, distance measured from the water surface.

Greek symbols

- α, thermal diffusivity, $k/\rho c$;
- γ, temperature gradient defined in equation (4);
- Δ, depth of interfacial entrainment layer, see Fig. 4;
- η, dimensionless mixed layer thickness, h/δ;
- δ, thickness of the surface skin layer;
- ε, long wave emissivity of water surface;
- θ, dimensionless temperature, $(T - \tilde{T}_a)/(T_{0i} - \tilde{T}_a)$;
- Γ, dimensionless stratification parameter; γ/γ_i;
- κ, factor defined in equation (9);
- ρ, density;
- σ, Stefan–Boltzmann constant;
- τ, dimensionless time, $\alpha t/\delta^2$.

Subscripts

- a, ambient air;
- i, initial time;
- m, mixed layer;
- 0, surface;
- s, top of the stable layer.

1. INTRODUCTION

FLUID motion induced by buoyancy forces arising as a result of fluid density variations are evident in a wide range of phenomena in physics, geophysics and engineering. Cooling of thermally stratified layers of fluid from above arises in many problems of interest. For example, the transport processes governing the vertical distribution of mass and energy in impounded waters (ponds, lakes and reservoirs) can play a critical role in various other basic and applied studies of current interest: in the use of large waterbodies for seasonal thermal energy storage [1], in the design of solar ponds [2], in the dispersal of material pollutants [3], in the transport of nutrients and biota [4,5], and on the dispersal of thermal effluents in cooling ponds and lakes [6].

The thermal structure in large bodies of water such as lakes and oceans has been discussed by Turner [7], and the field and empirical–analytical studies have been reviewed by Ryan [8], and there is no need to repeat these reviews. The convective processes below the water surface are very complex [7] and available experimental evidence indicates that the vertical temperature structure near the air–water interface is usually composed of several regions depending on different influences [9–11]. The water surface temperature is almost always cooler than the water a millimeter or so below it, except during intense insolation of quiescent waterbodies. This is due to the fact that the net heat transfer is usually upwards because the incident solar radiation which is a large fraction of the net heat input is absorbed in the interior of the water

and not at the surface [12]. At the very surface, heat is transported upwards by molecular processes within a very thin (1–3 mm) thermal boundary layer across which a relatively large temperature gradient exists [11].

The maintenance of stratification between the hot and cold fluid layers and the behavior of the hot–cold transition zone ("thermocline") in large scale, low temperature (below 100°C) thermal energy storage reservoirs for residential and for industrial processes is a new area of current concern [1,13]. The bulk of experimental work has been devoted to studying free convection in a thermally uniform layer of water being cooled from the free surface. A detailed experimental study of the steady temperature structure in the top-surface thermal boundary layer was reported by Katsaros *et al.* [14] using a traversing platinum film resistance probe, and the flow field was visualized using tracers which consisted of a rheoscopic fluid made from fish scales. They have also presented a thorough review of the relevant literature which will not be repeated here. A somewhat related study dealing with cooling of thermally stratified water from above, which was intended to simulate a large waterbody, has been reported by Dake and Harleman [10]. A tank containing initially stagnant, constant temperature water was first stratified by heating from an array of mercury and infrared lamps. The thermally stratified water was then allowed to cool naturally by exchanging heat with the laboratory environment. Vertical temperature profiles in the tank during the cooling were measured, but the growth of the mixed layer was not studied.

Laboratory modeling of atmospheric penetrative convection in a tank of water which was continuously and uniformly stratified was performed by Deardorff *et al.* [15] and Heidt [16]. The water was heated from the bottom by imposing a constant temperature boundary condition. This was accomplished by circulating a warm fluid through passages at the bottom of the tank. Deardorff *et al.* [15] in a careful experimental study have measured with resistance-wires and thermocouples the vertical profiles of horizontally averaged temperatures and heat fluxes and determined the mixed layer growth. The dynamics of the layer was observed by Heidt using a shadowgraph technique. Relatively simple mathematical models have been developed to predict the mixed layer growth in penetrative convection that yielded good agreement with the observations [15,16].

The phenomenon of natural convection in a thermally stratified layer of water cooled from the free surface has not received much detailed study. One factor contributing to the difficulties in developing predictive models for the thermal structure of natural waters is the lack of knowledge of internal physical transport processes such as mixing and energy transfer. Several energy transport processes must be taken into account simultaneously, and the sources and sinks of energy are not obvious [7]. Laboratory experiments are therefore necessary in order to gain pertinent quantitative data for improved understanding of the detailed physical processes of buoyancy driven convective mixing in fluids cooled from the free surface. The purpose of this work is to furnish experimental evidence on thermal and fluid kinetics in stratified water cooled from above under carefully controlled laboratory conditions and to analytically model the mixed layer dynamics. In the present experiments, stratification is induced by radiation to simulate solar heating, and after the heating has been terminated the water is then cooled from the free surface to model the cooling of natural waterbodies. The vertical temperature profiles are measured optically using a Mach–Zehnder interferometer and the growth of the mixed layer is determined. The diurnal and seasonal dynamics of the convective layer growth in waterbodies are of considerable practical interest in the seasonal storage of thermal energy, in the design of solar ponds, in the vertical pollutant, nutrient and biota transport and in the dispersal of thermal effluents in cooling ponds and lakes.

2. EXPERIMENTS

2.1. *Test apparatus and data reduction*

The observational data on the dynamics of mixed layer growth during cooling of thermally stratified water from above are very limited because of difficulties in realistically modeling the physical processes in the laboratory. The limitations of instrumentation requiring the presence of sensing elements within the water to determine the temperature distribution is also a contributing factor. In order to partially circumvent these difficulties in the present investigation, a Mach–Zehnder interferometer was selected as a diagnostic tool for measuring the unsteady temperature distribution. The Mach–Zehnder interferometer is an ideal instrument to study two-dimensional transport phenomena. If it is possible to align the axis of symmetry of the phenomena studied along the optical axis, then each fringe shift can be directly related to a change in the index of refraction of the fluid. A photograph of the fringe shifts in the test cell gives an instantaneous information of the field studied in the entire region. Since the system senses differences in the refractive index of water, it requires no physical contact of a foreign object with the fluid and does not disturb or distort the temperature field. Interferometry is considered to be the best method for obtaining quantitative temperature profiles [17]. The interferometer used in the study was of typical rectangular design with 25 cm dia optics. A He–Ne laser served as a light source, and a system of lenses with 25 cm dia parabolic mirrors produced a collimated beam.

A rectangular test cell with the inside dimensions of 10 cm along the optical path, 25 cm wide, and 40 cm deep, was placed in one leg of the interferometer. The optical glass windows, 2.5 cm thick, acted as walls. To insure that the windows were parallel, the sides and bottoms of the cell were machined together to 10 cm (± 0.013 cm) which insured a uniform width. Aluminum frames were placed over the outside of the

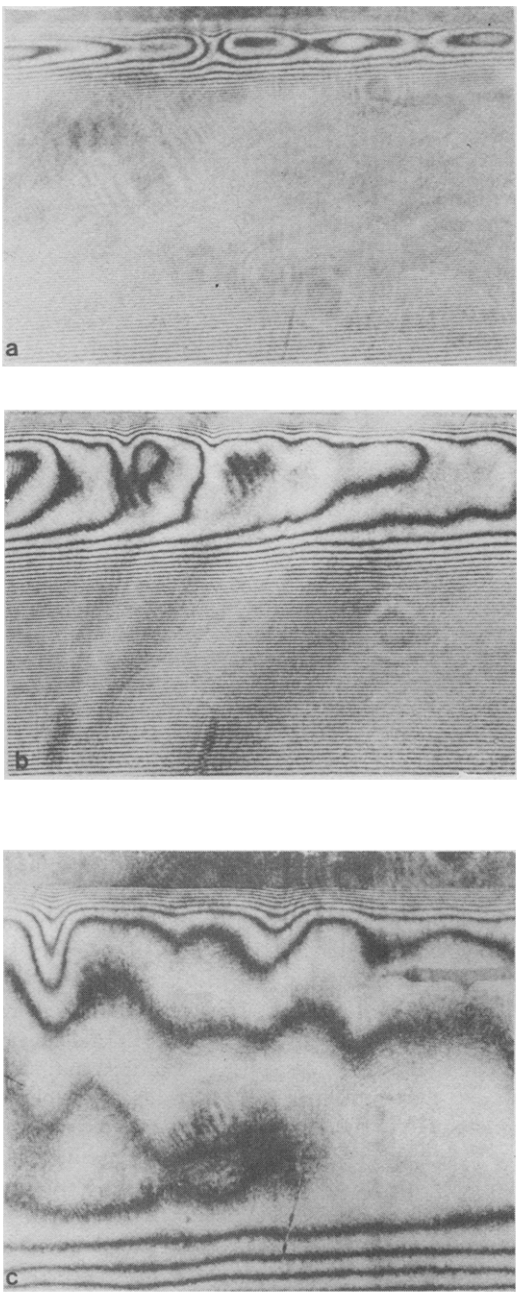

FIG. 1. Selected interferograms illustrating cooling of intensely stratified layer of water; heat exchange between the surface and environment, $T_a = 25°C$: (a) $t = 2$ min; (b) $t = 10$ min; (c) $t = 25$ min.

windows but supplied only enough force to counter the hydrostatic pressure. Urethane insulation was placed along the side walls and covered the optical windows. The insulation from the windows could easily be removed to take photographs of the interference fringe pattern.

The test cell was cleaned and then filled with distilled water, covered, and left undisturbed for some time to eliminate all convective currents which are normally present and to attain a uniform room temperature. The water was then thermally stratified using radiant heaters to a predetermined temperature level. The radiant heaters consisted of tungsten filament lamps in parabolic reflectors with known spectral radiation characteristics. The reflectors were designed to provide a collimated radiation beam within a 5 cm wide 25 cm long rectangular region. Two such side-by-side radiant heater units were used to irradiate the water in the test cell.

After the heating of the water was terminated, the water was allowed to cool freely by convective, latent and radiant heat exchange with the ambient air and surroundings. To control more effectively the "environment" temperature and the cooling rate than was possible with the free-cooling tests, the water could also be cooled by a copper heat sink which was placed above the water but not in direct contact with it. The temperature of the sink was controlled by circulating ethylene glycol through grooves milled in the copper block. At desired intervals, the interference fringe patterns were photographed with a 35 mm camera and reference as well as other thermocouple readings were simultaneously recorded.

The position of the interference fringes was measured using a vernier microscope that was accurate to ± 0.01 mm corresponding to an actual distance of approximately ± 0.015 mm. Subsequently, the interferograms were interpreted using the accurate relation between index of refraction and temperature data [18] to obtain the temperature profiles. A single reference temperature needed to interpret the interferograms was measured with a calibrated Type-K thermocouple. The data reduction procedure is discussed in detail elsewhere [11]. The estimated accuracy of the temperature measurement is about $\pm 0.06°C$.

2.2. *Qualitative discussion of some observational data*

Some typical photographs of the interference fringe patterns illustrating an intensely stratified water being cooled from the free surface by heat exchange with colder air and surroundings are shown in Fig. 1. Initially the surface temperature was about 22°C higher than the bulk temperature prior to stratification. Because of the large temperature gradients the fringe density was quite high and therefore difficult to interpret accurately. A short time after stratification was terminated and cooling was started, buoyancy driven convection developed. The convective flow in the water was confined to a small region near the interface and the mean temperature of the mixed layer (rather uniform temperature region about 2 mm below the surface) was higher than that of the stable region below. Figure 1a shows that the convection had a regularly structured circulation pattern with a cell spacing of about 1.8 cm which increased as the convective region became larger. The process was similar to that described by Berg *et al.* [19] and called vermiculated rolls. The roll pattern was observed to exist until the convective layer became approximately 2 cm deep, and then as the flow became turbulent the structure deteriorated (Fig. 1b). The resulting motion after the roll pattern eroded was characterized by plunging sheets of water which was similar in nature to

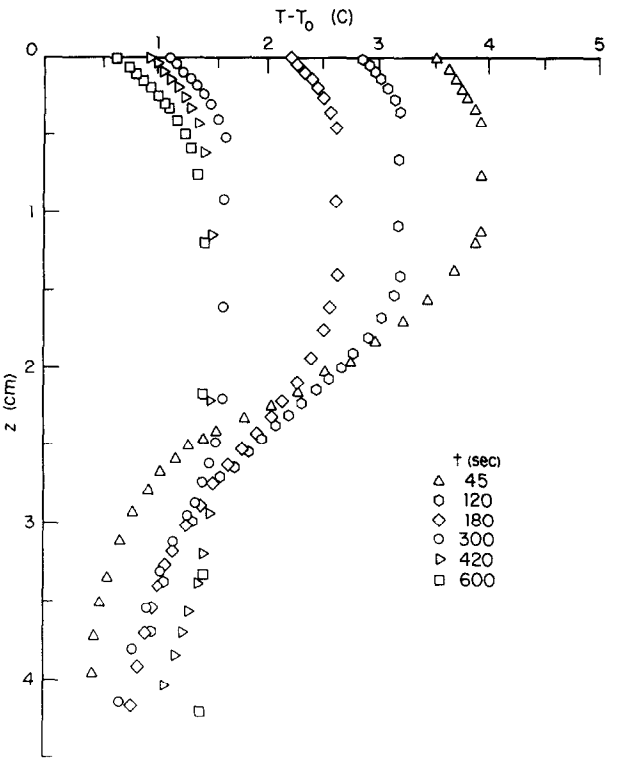

FIG. 2. Temperature distribution during cooling of thermally stratified water; heat exchange with a sink placed above the water surface, $T_{sink} \simeq 5.5°C$.

that described by Spangenberg and Rowland [20]. The vertical temperature profiles for a different experiment are shown in Fig. 2. In this experiment water was cooled from the free surface by a copper heat sink placed above the water surface but not in direct contact with it. The temperature profiles presented are similar to those that have been obtained for a number of experiments under different initial stratification and cooling conditions. The interferograms and the measured temperature profiles reveal that there is no overshoot at the bottom of the mixed layer (i.e. no injection of convective fluid into the top of the stable region). Other investigators [15,16] who have studied mixed layer growth in an initially uniformly stratified (i.e. linearly varying temperature with depth) water heated from below have noted a measurable overshoot. This difference may, in part, be due to the fact that in the present experiments the water was stratified nonuniformly (see Fig. 2 for $t = 45$ s) with the intensity of stratification decreasing with depth and that the turbulence was less intense.

The stable region below the mixed layer resisted the downward motion of the fluid and kept the circulation confined to a well defined layer near the surface. As the water cooled and the mean temperature of the mixed layer decreased, the convection penetrated deeper into the stable region. With continued cooling the depth of the mixed layer increased (Fig. 1c); eventually the stable region was completely penetrated by the convective layer. Both plumes and sheets of descending colder water were evident leaving the vicinity of the interface. The denser water would penetrate up to 15 cm into the underlying region before losing its thermal identity. The interferometer yields only a two-dimensional temperature field, and little can be said about the three-dimensional nature of the process of convection and mixing.

The visualization of the flow field in the mixed layer by the electrochemical dye technique [21] did not yield useful quantitative data. Because of the continuous, rather vigorous mixing it was very difficult to follow a streak of dye. The dye generated by pulsing electrical current through the platinum electrode mixed with the water in the convective layer and filled it completely. Figure 3 clearly shows that the flow is confined to the mixed layer and that there is an overshoot at the bottom of the layer. At this time during the experiment the circulation (roll) pattern is still regular and thus indicates that turbulence has not yet been fully established. Observations showed that the interface shape between the mixed and stable layers was highly irregular and undefinable. This observation is consistent with the results of Deardorff *et al.* [15] who found the interface to be a highly contorted region due to the physical overshooting into the stable region of energetic fluid elements which originate in the layers near the surface and continuously bombard the interface. The difference between interferometric and flow visualization observations result from the fact that the interferometer averages the temperature along the optical path. The almost undefinable interface between the mixed and the stable layers caused some difficulty in determining precisely the mixed layer depth. The mixed layer was considered to be the

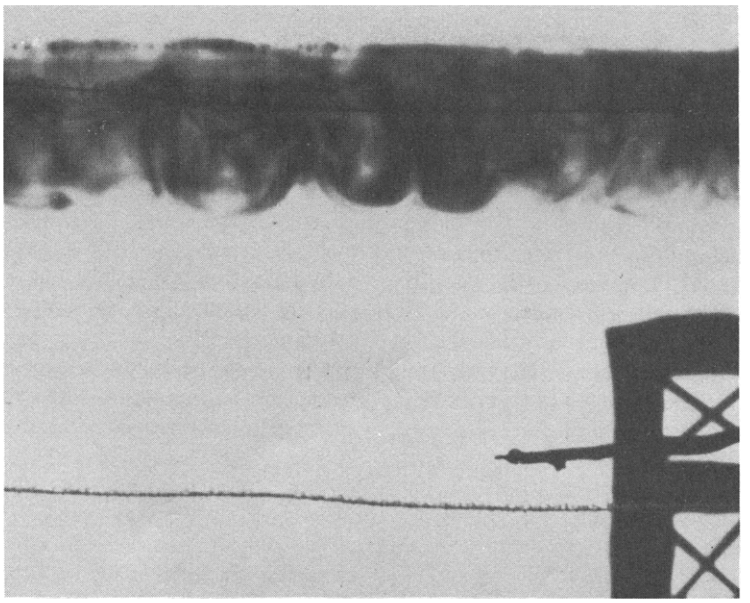

FIG. 3. Photograph illustrating mixing in the convective layer during cooling from the surface; $T_o = 21°C$, $T_{sink} \simeq 2°C$.

thickness of the largest cell or the largest vertical distance between two points on the same interference fringe in the mixed layer.

The experimental observations made during the cooling of thermally stratified water show complex vertical temperature structure which can be considered as consisting of several regions. Each of these regions is dependent upon different influences and energy transport processes. The region between the surface and the top of the mixed layer is referred to as the thermal boundary layer and is from about 1 to 4 mm thick. This layer includes the so-called skin layer which is about 0.2 mm thick. Energy transport in this layer is primarily by molecular conduction as sharp temperature gradients are evident from the interferograms. In the region between the skin and mixed layers ($0.2 < z < 4$ mm), which is referred to as the buffer layer, energy transport by molecular diffusion is of about the same order of magnitude as turbulent diffusion. Observations have shown that the thermal boundary layer was very persistent. The layer was shortly reestablished after being distorted, and its thickness grew at a very slow rate independent of the thermal conditions. The thickness of this layer appeared to be related to the size of the eddies and the scale of the turbulent motion. In the mixed layer, heat is transported primarily by buoyancy driven circulation and turbulent diffusion. Below the mixed layer is an interfacial layer where cold fluid is entrained by warmer fluid. The nonturbulent stable layer where $\partial T/\partial z < 0$ is below the entrainment layer. The depths of the layers indicated above are difficult to define precisely, and rigorous mathematical and physical requirements for them cannot be stated at the present time.

3. ANALYSIS

3.1. *Physical model and assumptions*

The vertical temperature structure in a developing convectively unstable surface layers of stratified water can be schematically represented as in Fig. 4. The thermal structure is considered to consist of four layers: surface thermal boundary layer, convective (mixed) layer, interfacial entrainment layer, and stable region. The thin thermal boundary layer develops rapidly and its thickness is assumed to be constant. Temperature gradients are large in this layer and heat is predominantly transported by molecular and turbulent diffusion. The thorough mixing in the free convective layer below the surface boundary layer is

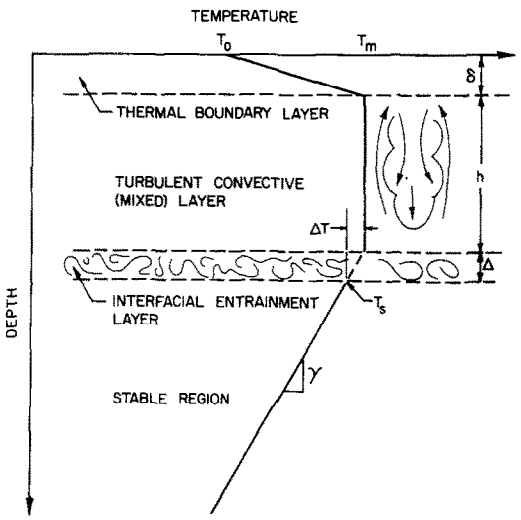

FIG. 4. Schematic representation of the developing unstable convective layer and the adopted temperature profile.

buoyancy dominated and is assumed to produce a temperature which is independent of depth. Two of the main factors controlling the development of the convective layer are the heat-transfer rate at the air–water interface and the turbulent mixing process which occurs at the interface between the well mixed convective layer of water and the water in the stable region below. Within the strongly agitated region, the interfacial entrainment layer of depth Δ, the temperature field is considered to have a marked spatial variation with the net effect being a change in temperature across the layer from the mixed layer value T_m to T_s at the top of the yet undisturbed stable region. The interfacial entrainment layer varies in depth and character; however, to facilitate the analysis it is assumed that the temperature change ΔT across the interfacial entrainment layer is proportional to its depth Δ.

The simple physical model described above is similar to the convectively unstable planetary boundary layer in the atmosphere capped by a stable layer. The essential details concerning the original development of the penetrative convection model are discussed by Plate [22]. More current contributions to the theory can be found in recent papers by Zeman and Tennekes [23] and by Venkatram and Viskanta [24] together with up-to-date reviews of the literature.

3.2. *Thermal model for dynamics of the mixed layer*

The layer of water is assumed to be a horizontally homogeneous incompressible fluid obeying the Boussinesq approximation [25] with energy transport in the vertical direction only. The viscous heat dissipation and internal radiation transfer are neglected. Making use of these approximations and the ones introduced in the previous subsection, the conservation of energy equation (i.e. the First Law of Thermodynamics) for an incompressible fluid reduces to

$$\rho c\left[\frac{\partial T}{\partial t}+\frac{\partial(\overline{w'T'})}{\partial z}\right]=k\frac{\partial^2 T}{\partial z^2}. \tag{1}$$

The term $\rho c\partial(\overline{w'T'})/\partial z$ represents the local divergence of the turbulent flux of heat. It is this term that contributes in a major way to redistribution of the heat exchanged at the air–water interface. Rearranging equation (1) yields

$$\frac{\partial T}{\partial t}=\frac{\partial}{\partial z}\left(\alpha\frac{\partial T}{\partial z}-\overline{w'T'}\right)=-\frac{1}{\rho c}\frac{\partial H}{\partial z}, \tag{2}$$

where

$$H=\rho c\left(\overline{w'T'}-\alpha\frac{\partial T}{\partial z}\right) \tag{3}$$

is the local heat flux at any depth z. In writing equation (1) it was assumed that the difference between the potential and the actual *in situ* thermodynamic temperature is negligible [25]. This assumption should be well justified for the experimental conditions.

Since the turbulent diffusion term in the energy equation cannot be readily evaluated, based on the experimental observations, the following additional simplifying assumptions are introduced: (1) the change in internal energy of the skin layer (thermal boundary layer) is negligible; (2) the turbulent diffusion predominates over the molecular diffusion in the mixed (convective) layer and the temperature in this region is independent of z; (3) the temperature decreases linearly in the stable region; and (4) the temperature at the bottom of the water body is constant.

The above assumptions provide considerable mathematical simplification and allow the mean temperature to be written as

$$T(z,t)=\begin{cases}T_0(t)+(z/\delta)[T_m(t)-T_0(t)], & 0<z<\delta\\ T_m(t), & \delta<z<\delta+h\\ T_s(t)+\gamma(t)[z-(\delta+h)], & z>\delta+h.\end{cases} \tag{4}$$

In most similar thermal models [16,26] the presence of the skin layer (thermal boundary layer) has been neglected. Substituting these approximations in the energy equation, equation (2) yields for the convective layer the equation

$$\frac{dT_m}{dt}=-\frac{1}{\rho c}\frac{\partial H}{\partial z}. \tag{5}$$

Integration of equation (5) with respect to z from $z=0$ to $z=\delta+h$ and making use of assumption 1, yields

$$h\rho c\frac{dT_m}{dt}=H(0,t)-H(h,t), \tag{6}$$

where $H(0,t)$ is the total heat flux at the water surface ($z=0$), and $H(h,t)$ is the heat flux at the bottom of the mixed layer ($z=\delta+h$). The heat flux at the water surface is the sum of the convective, latent, and radiative energy fluxes. The instantaneous energy balance at the interface can be expressed as

$$-k\left.\frac{\partial T}{\partial z}\right|_{z=0}=-H(0,t)=h_c(T_0-T_a)+\varepsilon\sigma(T_0^4-T_e^4)+g(p_0-p_a)h_{fg}. \tag{7}$$

An additional equation needed to evaluate the heat flux at the bottom of the convective layer can be obtained by making an assumption about the joining of the temperature profile at the "interface" between the stable region and the convective layer. Experimental evidence suggests entrainment of cool water into the mixed layer from the stable region. The relation between the heat flux and the temperature is formulated on the basis of the assumed or ideal temperature structure at the interfacial entrainment layer between the mixed layer and the stable region shown in Fig. 4. From an energy balance on the interfacial entrainment layer and the assumed temperature profile shown in Fig. 4, the time rate of change of the temperature difference ΔT can be expressed as

$$\frac{d\Delta T}{dt}=\frac{d(\gamma\Delta)}{dt}=\frac{d(\gamma h)}{dt}-\frac{dT_m}{dt}. \tag{8}$$

This relation simply states that the rate of change of ΔT depends on two different effects. It is increased by

entrainment (first term) and decreased by cooling (second term).

The entrainment of cold, stable water from below into the warmer mixed layer leads to a downward heat flux at the bottom of the layer. This heat flux can be expressed as

$$H(h,t) = -\rho c\Delta \frac{\mathrm{d}(\gamma h)}{\mathrm{d}t} = -\kappa(t)H(0,t). \quad (9)$$

The RHS of this equation provides a closure condition [26] for the problem and simply states that the heat transported into the mixed layer due to entrainment is proportional to the heat flux at the free surface. The approach of taking the heat flux at the top of the stable region to be proportional to the surface heat flux if the layer is in state of free convection is well established in the literature [24, 26, 27]. The proportionality factor κ lies between zero and unity and will be established from the experimental data.

Equation (7) can be rewritten as

$$-H(0,t) = (k/\delta)(T_m - T_0) = \tilde{h}(T_0 - \tilde{T}_a), \quad (10)$$

where the effective heat exchange coefficient, $\tilde{h}$, is defined as

$$\tilde{h} = \frac{h_c(T_0 - \tilde{T}_a) + h_{fg}g(p_0 - p_a) + \varepsilon\sigma(T_0^4 - T_e^4)}{(T_0 - \tilde{T}_a)}. \quad (11)$$

Since the temperature profile in the thermal boundary layer is assumed to be linear, see Fig. 4, the surface temperature T_0 can be related to the mean temperature T_m of the mixed layer. The justification of this assumption will be discussed later. From the energy balance at the interface, equation (10), there results

$$T_0 = [\tilde{h}\tilde{T}_a + (k/\delta)T_m]/[\tilde{h} + (k/\delta)]. \quad (12)$$

The set of coupled model equations, equations (6)–(12), describe the heat-transfer driven growth of the mixed layer. These general model equations are not expected to render analytical solution except in special instances. The solutions of these equations with the help of further simplifying assumptions are discussed in the next subsection.

3.3. *Model equations for the special case κ = constant*

It is fortunate that equations (6), (8) and (9) allow a simple quadrature. Substituting equation (8) into equation (6) to eliminate $\mathrm{d}T_m/\mathrm{d}t$, dividing the resulting expression by equation (9) and making use of the closure condition (9), we obtain

$$\frac{\mathrm{d}(\gamma\Delta)}{\mathrm{d}(\gamma h)} + \left(\frac{1+\kappa}{\kappa}\right)\left(\frac{\gamma\Delta}{\gamma h}\right) - 1 = 0. \quad (13)$$

The general solution of equation (13) for $\gamma \neq 0$ and κ = constant is

$$\gamma\Delta = C(\gamma h)^{-(\kappa+1)/\kappa} + \left(\frac{\kappa}{1+2\kappa}\right)(\gamma h). \quad (14)$$

If as according to Deardorff *et al.* [16] $\kappa \simeq 0.2$, then $(\kappa + 1)/\kappa = 6$. Because of the large powers of γh occurring in equation (14), $\gamma\Delta$ in this equation rapidly loses its dependence on the initial conditions. This result is reasonable as it indicates that entrainment is controlled primarily by the dynamics of turbulence (i.e. mixed layer depth h) and not by the initial conditions. Without too much loss in generality, assuming that $\gamma\Delta = 0$ when $\gamma h = 0$ yields

$$\gamma\Delta = \left(\frac{\kappa}{1+2\kappa}\right)\gamma h. \quad (15)$$

This equation requires that the depth of the entrainment layer Δ be a constant fraction $[\kappa/(1+2\kappa)]$ of the developing mixed layer depth h. The result is not explicitly dependent on κ, but does depend on κ being constant. The assumption of κ = constant can be relaxed and more general results can be obtained by adopting some of the ideas developed by Zeman and Tennekes [23] for the growth of the convective planetary boundary layer.

Substituting equations (9) and (10) into equation (6) gives

$$\rho ch\frac{\mathrm{d}T_m}{\mathrm{d}t} = (1+\kappa)H(0,t) = (1+\kappa)(T_0 - T_m)(k/\delta). \quad (16)$$

Similarly substituting equations (8) and (9) into equation (6), replacing $\gamma\Delta$ with the help of equation (15) and then making use of equation (10) in the resulting expression to eliminate $H(0,t)$ yields

$$\rho ch\frac{\mathrm{d}(\gamma h)}{\mathrm{d}t} = (1+2\kappa)(T_0 - T_m)(k/\delta). \quad (17)$$

There is a system of three equations, equations (16), (17) and (12) for the three unknowns: T_m, T_0 and h. These equations must be solved simultaneously with the initial conditions

$$\left.\begin{aligned} T_m &= T_{mi}, \quad \text{at} \quad t = t_i \\ \text{and} \qquad T_0 &= T_{0i}, \quad \text{at} \quad t = t_i \\ h &= h_i, \quad \text{at} \quad t = t_i. \end{aligned}\right\} \quad (18)$$

Since the equations are nonlinear, in general, only numerical solutions are possible.

If the instantaneous heat flux $H(0,t)$ is prescribed and not expressed in terms of the temperature difference $(T_0 - T_m)$ then substituting equation (8) into equation (6), replacing $\gamma\Delta$ with the help of equation (15) and then eliminating $H(h,t)$ with the help of equation (9) in the resulting expression yields

$$h\rho c\frac{\mathrm{d}(\gamma h)}{\mathrm{d}t} = \rho c\left[\tfrac{1}{2}\gamma\frac{\mathrm{d}h^2}{\mathrm{d}t} + h^2\frac{\mathrm{d}\gamma}{\mathrm{d}t}\right] = (1+2\kappa)H(0,t). \quad (19)$$

This equation can be integrated once the variation of γ with time is prescribed. For the special case of γ = constant, formal integration of equation (19) yields

$$h^2 = h_i^2 + 2\left(\frac{1+2\kappa}{\rho c\gamma}\right)\int_{t_i}^{t} H(0,\tau)\,\mathrm{d}\tau \quad (20)$$

with $h = h_i$ at $t = t_i$. Unfortunately, the heat flux at the air–water interface $H(0,t)$ is not known *a priori* but is defined in terms of the surface temperature T_0, equation (10), which in turn is given in terms of the mean temperature of the mixed layer T_m, equation (12). For the case of constant heat flux at the surface, $H(0,\tau) = H$, equation (20) shows that $h \propto t^{1/2}$. This is in agreement with the results of other investigators [15,

22, 27]. However, when the energy input into the water is by means of constant shear stress at the boundary rather than heat, at large times the mixed layer grows as $t^{1/3}$ instead of $t^{1/2}$ [28,29].

The model equations, equations (16), (17) and (12), can be rearranged into a dimensionless form as follows:

$$\eta \frac{d\Theta_m}{d\tau} = (1+\kappa)(\Theta_0 - \Theta_m), \tag{21}$$

$$\eta \frac{d(\Gamma\eta)}{d\tau} = (1+2\kappa)S(\Theta_m - \Theta_0), \tag{22}$$

and

$$\Theta_0 = \Theta_m \Big/ \left[1 + \left(\frac{\tilde{h}}{k/\delta}\right)\right]. \tag{23}$$

In summary, a model for predicting the growth of the convective layer has been formulated. The analysis is similar to the models developed to predict the height of the convective layer capped by a stable layer in the atmosphere and can be considered an application of and extension of those analyses [26,27]. The model takes into account both the cooling processes of the convective layer and entrainment of cold water into it from the stable region below, but the analysis has neglected the effect of wind stress at the water surface on the mixed layer growth.

Substitution of equation (23) into equations (21) and (22) results in a system of two ordinary differential equations. A fourth order Runge–Kutta method was used to solve the system of equations. The method requires a definite value for the derivative at the initial time ($\tau = 0$) in order to solve for the function after a time increment. Therefore, the singularity at $\tau = 0$ (i.e. $\eta = 0$ at $\tau = 0$) should be treated carefully in the numerical solution of the equations.

RESULTS AND DISCUSSION

4.1. *Prediction of the mixed layer growth*

Before discussing the results it is worthwhile to emphasize some of the limitations of the model used in the study. The laboratory and theoretical model is driven by heat exchange at the water surface, and wind shear at the water surface is absent. Modeling of the dynamics of the mixed layer in natural waterbodies would have to consider the presence of surface waves and wind stress at the water surface, absorption of solar radiation and possibly for potential and kinetic energy changes of the water [29,30]. Although the analysis has bypassed the difficult problem of modeling turbulence and predicting the eddy diffusivities, this has been at the expense of generality. The temperature profile shape had to be prescribed *a priori* and there is a loss of detail in the determined temperature distribution.

The dimensionless model equations, equations (21)–(23), indicate that there are two dimensionless parameters and an empirical constant κ which control the dynamics of the mixed layer. The model is driven by heat exchange at the air–water interface, and the dimensionless surface heat-exchange coefficient ($\tilde{h}\delta/k$) is an important parameter as it is a relative measure of heat transfer from the water surface to the ambient environment to that of heat transport across the thermal boundary layer. The heat-transfer resistance between the water surface and the air is the dominant one during the mixed layer growth in the laboratory experiments since typically $\tilde{h}\delta/k < 1$. Equation (22) indicates that the thickening of the mixed layer depends on the dimensionless stratification parameter S. This parameter represents a relative measure of the driving buoyancy force $[(T_{0i} - \bar{T}_a)/\delta]$ in the thermal boundary layer which produces the flow to the intensity of the stratification (γ_i) or opposing buoyancy force which resists the motion. The constant κ will be determined from experimental data.

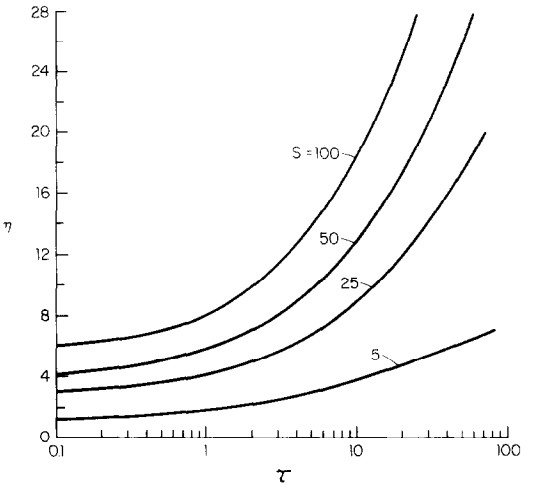

FIG. 5. Effect of the stratification parameter S on the dimensionless mixed layer thickness; $\kappa = 0.3$, $\tilde{h}\delta/k = 0.1$, $\Gamma = 1$.

The effect of the dimensionless stratification parameter on the mixed layer growth is illustrated in Fig. 5 for the case of time independent gradient Γ in the stable region. As expected, the results show that an increase in the parameter increases the growth rate. This indicates that the greater the stratification in the stable region, the more it resists the growth of the mixed layer. This finding is not surprising since the temperature gradient γ is proportional to the buoyancy force against which work must be done by the fluid parcels from the mixed layer.

The effect of the dimensionless heat transfer coefficient on the dimensionless mixed layer temperature (Θ_m) is illustrated in Fig. 6. It is noted from the figure that as the dimensionless heat-transfer coefficient increases the mean temperature of the mixed layer decreases more rapidly with time. This indicates that the higher the rate of heat loss from the surface, the more rapid is the cooling of the mixed layer. This is in agreement with expectations. Since the change of internal energy of the surface skin layer was neglected in developing the model equations, the change in the dimensionless surface heat-transfer coefficient produces the same effect on the surface temperature as it did on the mixed layer temperature.

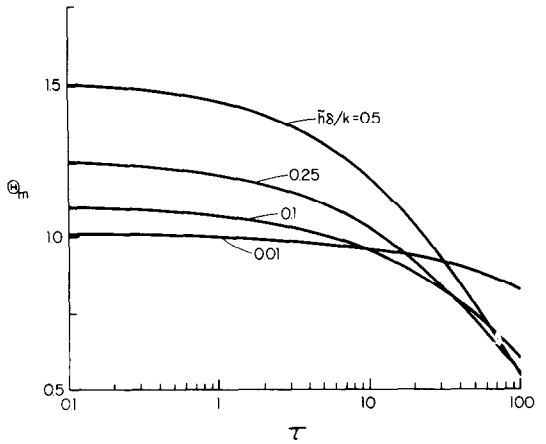

FIG. 6. Effect of parameter $\tilde{h}\delta/k$ on the dimensionless mean mixed layer temperature, $S = 50$, $\kappa = 0.3$, $\Gamma = 1$.

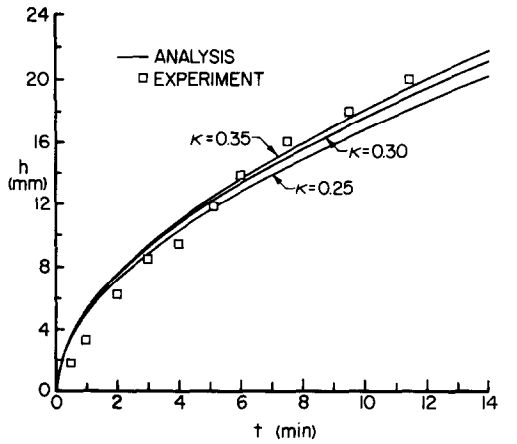

FIG. 7. Effect of parameter κ on the mixed layer thickness during cooling of thermally stratified water; heat exchange between the water and environment, $T_o = 17.5°C$, $T_a = 17.5°C$.

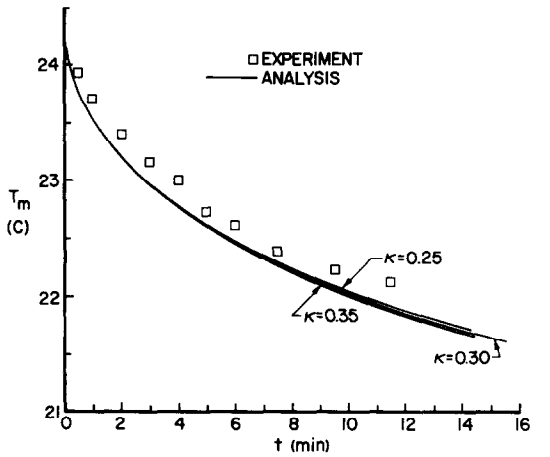

FIG. 8. Effect of parameter κ on the mean mixed layer temperature; see Fig. 7 for conditions.

4.2. *Comparison of model predictions with experimental data*

In the experiments performed, neither the temperature nor the heat flux at the water surface were constant. Therefore, as discussed before, the model equations could not be solved in closed form and numerical solutions were obtained. The effective heat-transfer coefficient $\tilde{h}$ was calculated from equation (11) for the experimental conditions. The proportionality factor κ which relates the heat flux at the water surface to the heat transported into the convective layer due to entrainment, see equation (9), was determined empirically using experimental data. The parameter is not constant during the development of the convective layer and varies with time, but in the calculations shown in Figs. 7 and 8 a mean value of κ was used. The results of Fig. 7 show that for small time ($t < 3$ min) h is rather insensitive to the value of κ. Because of the relative insensitivity of the results on κ and the uncertainty of its time dependence, a choice of a constant value is not likely to limit the range of applicability of the simple thermal model. The entrainment, however, is essentially a dynamic process and since the model does not treat adequately the entrainment in the interfacial region, this inadequacy may be one of the limitations of the model. In the results to be presented a constant average value of 0.3 was used in the computations. The value is in the range of constants cited in the literature [16] during the growth of the convective layer. In his experiments with water heated from below, Deardorff *et al.* [15] obtained time dependent values of κ ranging from 0.16 to 0.257. Heidt [16] found that κ is nearly constant and recommended a mean value of 0.18. The fact that for some short time after the cooling was initiated the buoyancy induced motion was laminar may partly explain the discrepancy between results reported in the literature and those obtained in this study as well as the disagreement between data and the predictions of the model indicated in Fig. 7. In this particular experiment it took approximately 3 min for the flow to become turbulent. In addition, for the present experiments the stratification was produced by radiation and was not uniform with depth. In contrast, the stratification was nearly uniform throughout the layer in the experiments of Deardorff *et al.* [15] and Heidt [16]. Finally, in this study the mixed layer growth was driven by cooling the water from the free surface while in the experiments of Deardorff *et al.* and of Heidt, the layer thickened because of heating from below at a solid boundary maintained at a constant temperature.

A comparison of the measured and predicted mixed layer thicknesses given in Fig. 7 shows that for short times ($t < 5$ min) the analysis overpredicts and for longer time ($t > 5$ min) underestimates the convective layer thickness. The overprediction of the mixed layer thickness is possibly due to the fact that early in the development of the convective layer the turbulence is not yet fully developed. The theoretical underestimation of T_m by about 10% (see Fig. 8) is considered to be due to inadequate modeling of the entrainment process. A change of κ from 0.3 to 0.2 would bring the measured and predicted temperatures to a better agreement, but the agreement between measured and predicted mixed layer depths would definitely be poorer for a $\kappa = 0.2$, at least for $t > 5$ min.

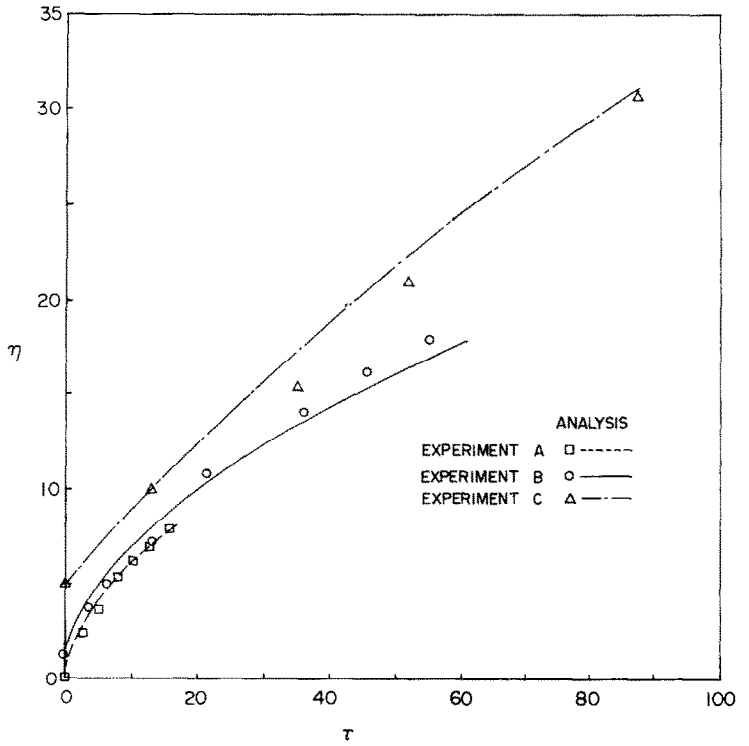

FIG. 9. Comparison of dimensionless mixed layer thickness between experiment and analysis; see Table 1 for conditions.

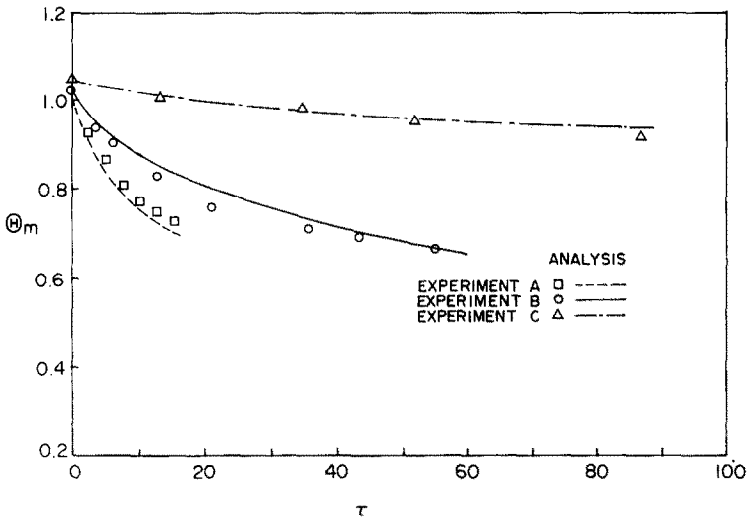

FIG. 10. Comparison of dimensionless mixed layer temperature between experiment and analysis; see Table 1 for conditions.

Table 1. The experimental conditions for different tests discussed

Exp.	T_0 (°C)	T_{0i} (°C)	T_a (°C)	T_{sink} (°C)	% Relative humidity	δ (mm)	γ_i (°C/cm)
A	18.0	23.8	18.0		75	2.5	−0.75
B	19.5	23.9	19.5		65	1.5	−0.68
C	22.0	26.8		5.8	60	1.0	−1.25

Figures 9 and 10 show the comparison between the measured and predicted dimensionless mixed layer thickness and mixed layer temperature, respectively. The experimental conditions for the different tests discussed here are summarized in Table 1. It should be mentioned that the thermal stratification for the experiments were different, and the cooling of the water continued until the mixed layer completely disappeared. The results for Experiments A and B (Fig. 9) reveal that the theoretically predicted η is somewhat higher than the experimental data at short times but lower at longer times. For Experiment C the theoretical predictions are in good agreement with the experimental data for short times and are about 10% higher for longer times. However, the results for the dimensionless mixed layer thickness (Fig. 10) show that the analysis consistently underpredicts the data by a few percent for Experiment A and overpredicts the data by about the same percentage for Experiment B. The dimensionless mixed layer temperatures predicted for Experiment C are in good agreement with observations for all times. In view of the approximate nature

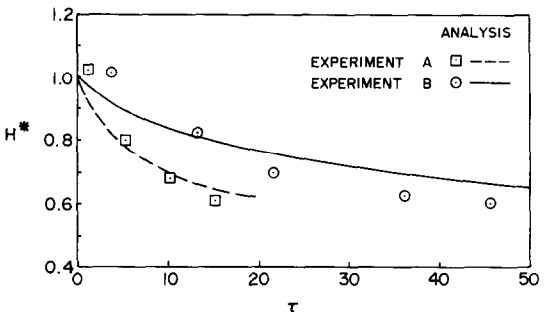

FIG. 11. Comparison of dimensionless surface heat flux between experiment and analysis; see Table 1 for conditions.

of the analysis and the inability to realistically model the entrainment process at the mixed layer-stable region interface, the agreement between predictions and data is encouraging and indicates that the model accounts for the essential physical processes.

The dimensionless heat flux predicted at the water surface, H^* [$= H(0,t)/\tilde{h}(\tilde{T}_a - T_{0i})$], is compared in Fig. 11 with the experimentally determined flux for two different experiments. The results show that the theoretically predicted H^* is lower than the experimental data for short times and is higher for longer times. This indicates that linearization of the interface energy balance by introducing a constant effective heat-transfer coefficient $\tilde{h}$ is not completely satisfactory. The value of $\tilde{h}$ is not constant but varies with time because of the nonlinear dependence of the convective, latent, and radiative heat transfer at the interface on the water surface temperature.

The comparison between the measured and the predicted mixed layer thickness calculated from equation (16) using an average value of the heat flux at the surface $\bar{H}(0)$ were made and results are presented elsewhere [11]. The results reveal that in order to obtain good agreement between the approximate analysis and the experimental data, the mean heat flux at the surface should be considerably lower than the predicted average heat flux obtained from Fig. 11. The discrepancy between the results indicates that the heat flux at the surface cannot be adequately represented by a mean value in predicting the mixed layer growth. It should be pointed out that a mean value of the thermal boundary-layer thickness δ was used in the theoretical predictions. The experimental data clearly show that the thermal boundary-layer thickness δ is not constant but increases with time particularly during the early stages of the mixed layer growth, see Fig. 2. However, the thermal resistance to heat transfer across the thermal boundary layer is small compared to the effective resistance to heat transfer on the air side of the water, and therefore the results of T_0, T_m, and h are relatively insensitive to the value of the thermal boundary-layer thickness δ used.

5. CONCLUSIONS

The simple thermal model developed predicts the dynamics of the convective layer. The model determines the thickness and mean temperature of the mixed layer as well as the surface heat flux. The thickness and the mean temperature of the mixed layer predicted by the model are, in general, within 10% of the observed results. The discrepancy is partially due to improperly modeling the entrainment process in the interfacial entrainment layer.

The accuracy of the predicted thickness and mean temperature of the mixed layer depend strongly on the surface thermal resistance on the air side but not so much on the thickness of the surface skin layer. However, accurate determination of the surface skin layer thickness is necessary for predicting the surface temperature.

The results obtained contribute some data and understanding necessary in developing much needed deterministic models for predicting thermal characteristics in complex hydraulic systems. Such models are needed for predicting vertical pollutant, nutrient and biota transport and predicting dispersal of thermal effluents in natural waterbodies, for the design of solar ponds and of seasonal thermal energy storage in large lakes. However, the knowledge of turbulent buoyant convection in nonuniformly stratified water and of the entrainment process between the unstable and stable regions in the water is incomplete for development of such models. Laboratory studies using much larger test cells and field experiments should be conducted to obtain needed data. A model for the dynamics of mixed layer growth in thermally stratified natural waterbodies should be developed by considering processes not accounted in the laboratory experiments and by relaxing some of the more restrictive assumptions made in the analysis.

Acknowledgements—This work was supported in part by the U.S. Department of Interior, Office of Water Research and Technology, through the Water Resources Research Center of Purdue University under the matching grant project OWRT-B-77-IND.

REFERENCES

1. G. Schöll, Warmwasser-Grosswärmespeicher, *Z. Ver. Dt. Ing.* **223**, 33–38 (1974).
2. A. Rabl and C. E. Nielsen, Solar ponds for space heating, *Solar Energy* **17**, 1–15 (1975).
3. J. L. Hamelnik and R. D. Waybrant, Factors controlling the dynamics of nonionic synthetic organic chemicals in aquatic environments, Purdue University, Water Resources Research Center, Technical Report No. 44 (1973).
4. D. W. Schindler and E. J. Fee, Diurnal variation of dissolved inorganic carbon and its use in estimating primary production, *J. Fish. Res. Bd. Can.* **30**, 1501–1510 (1973).
5. O. Holm-Hansen, R. Goldman, R. Richards and P. M. Williams, Chemical and biological characteristics of a water column in Lake Tahoe, *Limnol. Oceanogr.* **21**, 548–562 (1976).
6. F. K. Moore and Y. Jaluria, Thermal effects of power plants on lakes, *J. Heat Transfer* **94**, 163–168 (1972).
7. J. S. Turner, *Buoyancy Effects in Fluids*. Harvard University Press, Cambridge, Mass. (1973).
8. P. J. Ryan, Temperature distribution in lakes and reservoirs, in *Engineering Aspects of Heat Disposal from Power Generation*, summer short course notes, Chapter 2, pp. 2-1 to 2-80. Dept. Civil Engng, Mass. Inst. Technology, Cambridge, Mass. (1972).
9. E. D. McAlister and W. McLeish, Heat transfer in the top millimeter of the ocean, *J. Geophys. Res.* **74**, 3408–3414 (1969).
10. J. M. K. Dake and D. P. Harleman, Thermal stratification in lakes: Analytical and experimental studies, *Water Resour. Res.* **5**, 484–495 (1969).
11. R. Viskanta, D. M. Snider and M. Behnia, Laboratory modeling of thermal structure in stagnant water, Purdue University, Water Resources Research Center, Technical Report No. 62 (1975). (Available from NTIS, U.S. Department of Commerce, PB No. 245763.)
12. R. Viskanta and J. S. Toor, Radiant energy transfer in waters, *Water Resour. Res.* **8**, 595–608 (1973).
13. H. J. Leyers, F. Scholz and A. Tholen, Analytical and experimental determination of the temperature distribution in stratified hot water stores, 1977 International Seminar on Heat Transfer in Buildings, Dubrovnik, Yugoslavia (29 August–2 September 1977).
14. K. B. Katsaros, W. T. Liu, J. A. Businger and J. E. Tillman, Heat transport and thermal structure in the interfacial boundary layer measured in an open tank of water in turbulent free convection, *J. Fluid Mech.* **83**, 311–335 (1977).
15. J. W. Deardorff, G. E. Willis and D. K. Lilly, Laboratory investigation of nonsteady penetrative convection, *J. Fluid Mech.* **35**, 7–31 (1969).
16. F. D. Heidt, Comparison of laboratory experiments on penetrative convection with measurements in nature, in *Heat Transfer and Turbulent Buoyant Convection*, Vol. I, pp. 199–210, edited by D. B. Spalding and N. Afgan. Hemisphere, Washington, D.C. (1977).
17. W. Hauf and U. Grigull, Optical methods in heat transfer, in *Advances in Heat Transfer*, Vol. 6, pp. 191–362, edited by J. P. Hartnett and T. F. Irvine, Jr. Academic Press, New York (1970).
18. L. W. Tilton and J. K. Taylor, Refractive index and dispersion of distilled water for visible radiation at temperature 0 to 60°C, *J. Res. Nat. Bur. Stand.* **20**, 419–477 (1938).
19. J. C. Berg, A. Acrivos and M. Boudart, Evaporative convection, in *Advances in Chemical Engineering*, Vol. 6, pp. 61–123, edited by T. B. Brew, J. W. Hoopes, Jr. and T. Vermeulen. Academic Press, New York (1966).
20. W. G. Spangenberg and W. R. Rowland, Convective circulation of water induced by evaporative cooling, *Physics Fluids* **6**, 743–750 (1961).
21. D. J. Baker, A technique for the precise measurement of small fluid velocities, *J. Fluid Mech.* **26**, 573–575 (1966).
22. E. J. Plate, *Aerodynamic Characteristics of Atmospheric Boundary Layers*. U.S. Atomic Energy Commission, Oak Ridge, Tenn. (1971).
23. O. Zeman and H. Tennekes, Parametrization of the turbulent energy budget at the top of the daytime atmospheric boundary layer, *J. Atmos. Sci.* **34**, 111–123 (1977).
24. A. Venkatram and R. Viskanta, Effects of aerosol-induced heating of the convective boundary layer, *J. Atmos. Sci.* **34**, 1918–1933 (1977).
25. O. M. Phillips, *The Dynamics of the Upper Ocean*. Cambridge University Press, Cambridge (1966).
26. D. J. Carson and F. B. Smith, Thermodynamic model for the development of a convectively unstable boundary layer, in *Turbulent Diffusion in Environmental Pollution—Advances in Geophysics*, Vol. 18A, pp. 111 124, edited by F. N. Frankiel and R. E. Munn. Academic Press, New York (1974).
27. H. Tennekes, A model for the dynamics of the inversion above a convective boundary layer, *J. Atmos. Sci.* **30**, 558–567 (1973).
28. H. Kato and O. M. Phillips, On the penetration of a turbulent layer into a stratified fluid, *J. Fluid Mech.* **37**, 643–655 (1969).
29. K. L. Denman, A time-dependent model of the upper ocean, *J. Phys. Ocean.* **3**, 173–184 (1973).
30. G. L. Mellor and P. A. Durbin, The structure and dynamics of the ocean surface mixed layer, *J. Phys. Ocean.* **5**, 718–728 (1975).

CONVECTION NATURELLE DANS L'EAU THERMIQUEMENT STRATIFIEE PAR REFROIDISSEMENT SUPERIEUR

Résumé On étudie la cinétique et la thermique d'une couche d'eau pendant le refroidissement à partir de la surface libre et thermiquement stratifiée, en considérant la convection le transport d'énergie latente et le rayonnement. Des expériences de laboratoire sont faites et on utilise un interféromètre Mach–Zehnder pour mesurer la distribution non-stationnaire de température dans une cellule remplie d'eau préalablement stratifiée. On développe un modèle simple basé sur le bilan d'énergie pour prédire l'épaisseur et la température moyenne de la couche. Les résultats du calcul s'accordent à 10% près avec les résultats expérimentaux. On trouve que la solution numérique du modèle s'accorde mieux avec l'expérience que les solutions analytiques supposant un flux thermique constant sur la surface. On montre que la condition à la surface et les mécanismes physiques internes de mélange et d'entrainement doivent être mieux compris de façon à modéliser la dynamique de la couche de mélange dans les volumes naturels d'eau.

FREIE KONVEKTION IN VON OBEN GEKÜHLTEM, THERMISCH GESCHICHTETEN WASSER

Zusammenfassung—Die durch Konvektion, latenten Energietransport und Strahlung erzeugte Wärme- und Flüssigkeitsbewegung in der konvektiven Schicht von thermisch geschichtetem Wasser bei Abkühlung durch die freie Oberfläche wird untersucht. Es wurden Laborversuche durchgeführt und ein Mach-Zehnder Interferometer benutzt, um die instationäre Temperaturverteilung in einer mit anfänglich geschichtetem Wasser gefüllten Testzelle zu messen. Ein einfaches, auf thermischer Energiebilanz basierendes mathematisches Modell wird entwickelt, um die Dicke und die mittlere Temperatur der Schicht zu berechnen. Die Modellrechnungen stimmetn innerhalb von 10% mit den Ergebnissen entsprechender Laborversuche überein. Es zeigte sich, daß die numerische Lösung der Modellgleichungen mit den Meßdaten besser übereinstimmt als jene Ergebnisse, die auf der geschlossenen Form der analytischen Lösung bei Verwendung des konstanten mittleren Wärmestroms durch die Oberfläche basieren. Es zeigte sich, daß die Oberflächenrandbedingung und die inneren physikalischen Misch- und Bewegungsvorgänge besser verstanden werden müssen, um Modelle für das dynamische Verhalten der Mischungsschicht natürlicher Gewässer aufstellen zu können.

СВОБОДНАЯ КОНВЕКЦИЯ В ТЕРМИЧЕСКИ СТРАТИФИЦИРОВАННОМ ОБЪЁМЕ ВОДЫ, ОХЛАЖДАЕМОМ СВЕРХУ

Аннотация — Исследуется тепловая и динамическая кинетика конвективного слоя при охлаждении свободной поверхности термически стратифицированного объёма воды за счёт конвекции, скрытой теплоты и излучения. В проведенных лабораторных опытах интерферометр Маха-Цендера использовался для измерения нестационарного распределения температуры в экспериментальной ячейке, заполненной предварительно стратифицированным объёмом воды. Для расчёта толщины и средней температуры слоя разработана простая математическая модель, основанная на балансе составляющих тепловой энергии. Расчёты с помощью модели в пределах 10% согласуются с данными проведенных лабораторных экспериментов. Найдено, что численное решение модельных уравнений даёт лучшее совпадение с экспериментальными данными, чем аналитическое решение в замкнутой форме, использующее постоянный средний тепловой поток на поверхности. Сделан вывод о том, что для моделирования динамики слоя смешения в естественных водоёмах необходимо лучшее понимание граничного условия на поверхности и внутренних физических процессов смешения и уноса.